

Calibration-free quantification of absolute oxygen saturation based on the dynamics of photoacoustic signals

Jun Xia, Amos Danielli, Yan Liu, Lidai Wang, Konstantin Maslov, and Lihong V. Wang*

Optical Imaging Laboratory, Department of Biomedical Engineering, Washington University in St. Louis,
One Brookings Drive, Saint Louis, Missouri 63130, USA

*Corresponding author: lhwang@wustl.edu

Received May 17, 2013; accepted June 29, 2013;
posted July 3, 2013 (Doc. ID 190637); published July 29, 2013

Photoacoustic tomography (PAT) is a hybrid imaging technique that has broad preclinical and clinical applications. Based on the photoacoustic effect, PAT directly measures specific optical absorption, which is the product of the tissue-intrinsic optical absorption coefficient and the local optical fluence. Therefore, quantitative PAT, such as absolute oxygen saturation (sO_2) quantification, requires knowledge of the local optical fluence, which can only be estimated through invasive measurements or sophisticated modeling of light transportation. In this Letter, we circumvent this requirement by taking advantage of the dynamics in sO_2 . The new method works when the sO_2 transition can be simultaneously monitored with multiple wavelengths. For each wavelength, the ratio of photoacoustic amplitudes measured at different sO_2 states is utilized. Using the ratio cancels the contribution from optical fluence and allows calibration-free quantification of absolute sO_2 . The new method was validated through both phantom and *in vivo* experiments. © 2013 Optical Society of America

OCIS codes: (100.6950) Tomographic image processing; (110.5120) Photoacoustic imaging; (170.1460) Blood gas monitoring; (170.3880) Medical and biological imaging; (110.5125) Photoacoustics.

<http://dx.doi.org/10.1364/OL.38.002800>

Quantification of blood oxygen saturation (sO_2) is of great importance in preclinical and clinical imaging. For instance, real-time monitoring of cerebral sO_2 is valuable in the diagnosis of cerebral desaturations and vasospasm in stroke patients [1], and tumor hypoxia is strongly associated with tumor propagation and malignant progression [2]. Many techniques have been developed to quantify sO_2 *in vivo*; however, they all have limitations. For instance, near-infrared spectroscopy (NIRS) and diffuse optical tomography (DOT) lack the spatial resolution to differentiate heterogeneities in tumor oxygenation; functional magnetic resonance imaging monitors the blood oxygen level dependent (BOLD) contrast, which is sensitive only to deoxygenated hemoglobin; and positron emission tomography (PET) requires the use of ionizing radioisotopes [3].

Photoacoustic tomography (PAT) aims to overcome the aforementioned limitations. In PAT, tissue chromophores, such as oxygenated hemoglobin (HbO_2) and deoxygenated hemoglobin (Hb), absorb optical energy and emit acoustic waves that are detected by ultrasound transducers. The conversion of light to acoustic waves allows PAT to image structures in deep tissues with acoustically defined high spatial resolution [4–6]. Because the photoacoustic signal originates from specific optical absorption in units of J/m^3 , quantitative photoacoustic imaging of the optical absorption coefficient in units of m^{-1} requires knowledge of the local fluence in units of J/m^2 (F). However, due to the optical heterogeneities in tissue, quantification of F is challenging. Over the past few years, multiple methods have been proposed to address the problem [7]. For instance, Laufer *et al.* introduced a model-based inversion algorithm that can quantify chromophore concentrations when the target geometry is known [8], Bauer *et al.* combined DOT with PAT to assist in fluence quantification [9], and

Guo *et al.* proposed a frequency-domain method that took advantage of the fluence-independent acoustic spectra [10]. However, most of these methods require sophisticated modeling of optical and acoustic transportations, producing challenges for real-time imaging. Here, we propose a dynamic quantification method that can derive the absolute sO_2 value when its change is localized and can be simultaneously monitored with multiple wavelengths. The new method cancels the fluence effect based on the change of photoacoustic amplitude at each wavelength.

Photoacoustic amplitude is proportional to the initial pressure rise (p_0), which is the product of the Grüneisen coefficient (Γ), the optical absorption coefficient (μ_a), and the local fluence (F):

$$p_0 = \Gamma \mu_a F. \quad (1)$$

For visible and near-infrared light, the main absorbers in a blood vessel are oxygenated hemoglobin (HbO_2) and deoxygenated hemoglobin (Hb). Therefore, the optical absorption coefficient at wavelength λ_1 and sO_2 state a can be expressed as

$$\mu_a(\lambda_1, sO_2(a)) = \ln(10)[C_{HbT} \cdot sO_2(a) \cdot \varepsilon_{HbO_2}(\lambda_1) + C_{HbT} \cdot (1 - sO_2(a)) \cdot \varepsilon_{Hb}(\lambda_1)], \quad (2)$$

where C_{HbT} is the total hemoglobin concentration, and ε_{HbO_2} and ε_{Hb} are the molar extinction coefficients of HbO_2 and Hb, respectively. As Γ is independent of the optical wavelength, the ratio of the photoacoustic amplitudes probed at two wavelengths can be written as

$$\frac{PA(\lambda_1, sO_2(a))}{PA(\lambda_2, sO_2(a))} = \frac{C_{HbT}(a)[sO_2(a) \times \epsilon_{HbO_2}(\lambda_1) + (1 - sO_2(a)) \times \epsilon_{Hb}(\lambda_1)]F(\lambda_1)}{C_{HbT}(a)[sO_2(a) \times \epsilon_{HbO_2}(\lambda_2) + (1 - sO_2(a)) \times \epsilon_{Hb}(\lambda_2)]F(\lambda_2)}. \quad (3)$$

Because the local fluence is difficult to quantify, in the conventional approach, the ratio of the surface fluences at λ_1 and λ_2 is used as an approximation. Therefore the conventional approach assumes that the optical attenuation coefficients at two wavelengths are the same (Assumption A). Based on this assumption, $sO_2(a)$ can be derived from Eq. (3).

When there is a dynamic change in sO_2 , we can exploit the variation in photoacoustic amplitude at each wavelength. For an sO_2 change from state a to b , the ratio between the photoacoustic amplitudes measured at the two states can be written as

$$\frac{PA(\lambda_1, sO_2(a))}{PA(\lambda_1, sO_2(b))} = \frac{C_{HbT}(a)[sO_2(a) \times \epsilon_{HbO_2}(\lambda_1) + (1 - sO_2(a)) \times \epsilon_{Hb}(\lambda_1)]F(\lambda_1, a)}{C_{HbT}(b)[sO_2(b) \times \epsilon_{HbO_2}(\lambda_1) + (1 - sO_2(b)) \times \epsilon_{Hb}(\lambda_1)]F(\lambda_1, b)}. \quad (4)$$

When the local fluence does not change during the transition, i.e., $F(\lambda_1, a) = F(\lambda_1, b)$ (Assumption B), it can be canceled from Eq. (4), resulting in

$$\frac{PA(\lambda_1, sO_2(a))}{PA(\lambda_1, sO_2(b))} = \frac{C_{HbT}(a) sO_2(a) \times \epsilon_{HbO_2}(\lambda_1) + (1 - sO_2(a)) \times \epsilon_{Hb}(\lambda_1)}{C_{HbT}(b) sO_2(b) \times \epsilon_{HbO_2}(\lambda_1) + (1 - sO_2(b)) \times \epsilon_{Hb}(\lambda_1)}. \quad (5)$$

To solve the three unknowns in Eq. (5), $C_{HbT}(a)/C_{HbT}(b)$, $sO_2(a)$, and $sO_2(b)$, one needs to monitor the change in sO_2 using at least three wavelengths. In a simplified case, when the total hemoglobin concentration (C_{HbT}) does not change—i.e., $C_{HbT}(a)/C_{HbT}(b) = 1$ —imaging at two wavelengths suffices.

Both the conventional method and the new dynamic method require certain assumptions. We can examine which assumption is more easily fulfilled in deep tissue imaging with red and near-infrared light. Due to differences in optical scattering and absorption coefficients at different wavelengths, Assumption A can rarely be satisfied in deep tissues. In contrast, Assumption B can easily be satisfied if the sO_2 change is small and localized, e.g., within a blood vessel or a tumor region. Even when the sO_2 change is systemic, Assumption B may still apply if the imaging region is covered by tissue with little blood. When light propagates through the intervening tissue, the main attenuation mechanisms will be scattering and absorption from other intrinsic absorbers, such as melanosomes and water; therefore, the sO_2 change will have negligible influence. In comparison, Assumption A still fails in this case if the two imaging wavelengths are far apart, carrying distinct optical scattering and absorption coefficients.

When the sO_2 change is large, Assumption B may no longer be valid. To reveal how the two sO_2 calculation methods are affected, we performed Monte Carlo simulations [11]. The simulation geometry is illustrated in Fig. 1(a): we modeled a 300 μm diameter blood vessel embedded in a piece of tissue, illuminated from the

top by a uniform laser beam. Because the blood vessel is much smaller than tissue, the tissue is treated as a semi-infinite medium in the simulation. We studied four cases (four sO_2 -state pairs): 90%–10%, 90%–30%, 90%–50%, and 90%–70%. The sO_2 changes were monitored using two optical wavelengths: 650 nm ($\epsilon_{Hb}/\epsilon_{HbO_2} = 10.1$) and 750 nm ($\epsilon_{Hb}/\epsilon_{HbO_2} = 2.7$). The optical parameters for the blood and tissue were assigned according to [12,13]. Figure 1(b) shows the sO_2 values calculated using the dynamic and conventional methods. In general, the dynamic method is more accurate, especially when the sO_2 change is small. For the largest sO_2 change (from

90% to 10%), Assumption B is no longer valid (fluence changes 25% at 650 nm and 7% at 750 nm), yielding inaccurate sO_2 estimations. However, Assumption A is impacted more severely. Because the conventional method is based on static calculation, it is more vulnerable to the fluence change at the low sO_2 level. In contrast, the dynamic method utilizes the ratio of signals at two different states, allowing it to tolerate change more. Therefore, the dynamic method still gives a more

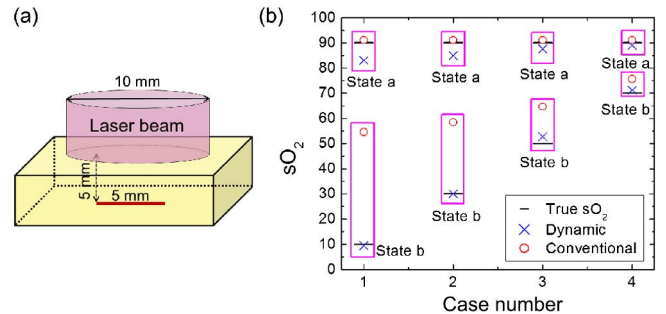


Fig. 1. (a) Physical model: a blood vessel embedded in a piece of tissue. (b) sO_2 values calculated using the dynamic and conventional methods. The simulation parameters are as follows: $\epsilon_{HbO_2}(650 \text{ nm}) = 368 \text{ cm}^{-1} \text{ M}^{-1}$, $\epsilon_{Hb}(650 \text{ nm}) = 3750 \text{ cm}^{-1} \text{ M}^{-1}$, $\epsilon_{HbO_2}(750 \text{ nm}) = 518 \text{ cm}^{-1} \text{ M}^{-1}$, $\epsilon_{Hb}(750 \text{ nm}) = 1405 \text{ cm}^{-1} \text{ M}^{-1}$, $C_{HbT} = 2.3 \text{ mM}$, $\mu_{atissue}(650 \text{ nm}) = 0.1 \text{ cm}^{-1}$, and $\mu_{atissue}(750 \text{ nm}) = 0.08 \text{ cm}^{-1}$. Scattering coefficients: $\mu_{sblood}(650 \text{ nm}) = 750 \text{ cm}^{-1}$, $\mu_{sblood}(750 \text{ nm}) = 720 \text{ cm}^{-1}$, $\mu_{stissue}(650 \text{ nm}) = 100 \text{ cm}^{-1}$, and $\mu_{stissue}(750 \text{ nm}) = 80 \text{ cm}^{-1}$. Anisotropy factors: $g_{blood} = 0.9945$ and $g_{tissue} = 0.9$.

reasonable estimation even when the sO_2 change is large. It is also worth mentioning that our simulation is based on human breast tissue, which has similar attenuation coefficients at 650 and 750 nm. In other biological tissues, the dynamic method could be even more advantageous.

To validate our model, we used a photoacoustic-computed tomography (PACT) system equipped with a 512-element ultrasound transducer array [14,15]. A schematic of the system is shown in Fig. 2(a). For simultaneous multiwavelength imaging, we combine an optical parametric oscillator (OPO) laser and a Ti:sapphire laser, each pumped by a Nd:YAG laser with a 10 Hz pulse repetition rate. The flashlamps in the two pump lasers are synchronized. By adjusting the delay between flashlamp and Q-switch firings, we make the OPO laser fire shortly after the Ti:sapphire laser, with a 72 μs delay. The two laser beams are combined with a dichroic mirror, and their incident fluences are measured by a laser power meter before the experiment. The photoacoustic signal is acquired by a 64-channel data acquisition (DAQ) system with a 40 MHz sampling rate. Once triggered by the Ti:sapphire laser, the DAQ system can continuously sample 4096 points, covering a span of 102 μs . Because the laser light also induces photoacoustic signals on the transducer surface, we can extract the exact firing time and the transducer's impulse response [white arrows, Fig. 2(b)]. The raw channel data is first deconvolved with Wiener deconvolution to remove the transducer's impulse response, and then reconstructed using the universal backprojection algorithm [16]. In all experiments, the wavelength of the OPO laser is set to 650 nm, and the wavelength of the Ti:sapphire laser is set to 750 nm.

The dynamic method was first validated through a phantom study. To mimic a blood vessel, we used a 300 μm inner diameter Silastic tube, covered by a 5 mm thick layer of chicken breast tissue. The two ends

of the tube were kept open to permit sequential flushing with venous and arterial defibrinated bovine blood. Before the experiment, the two blood samples were imaged at 798 nm, an isosbestic wavelength for HbO₂ and Hb absorption, and their photoacoustic amplitudes were found to be similar (<2% difference). This similarity ensured that the two blood samples had nearly the same total hemoglobin concentration, and thus two wavelengths were sufficient for sO_2 calculation. The sO_2 values of the two blood samples were measured beforehand using a blood gas analyzer (Stat profile pHox plus, Nova Biomedical) and found to be 90.1% (for arterial blood) and 63.6% (for venous blood), respectively. During the experiment, the tube was originally filled with arterial blood and then sequentially flushed with venous blood, arterial blood, and venous blood. Figure 3(b) and Media 1 show the change in average photoacoustic amplitude in the tube over time. The sO_2 value was calculated using the conventional method and the new dynamic method. The results, shown in Fig. 3(c) and Media 2, demonstrate that the dynamic method provides similar sO_2 values to the ones originally obtained from the blood gas analyzer. In contrast, the conventional method overestimates the sO_2 value. The results are consistent with our simulation studies. It can also be noticed that the sO_2 readings from the dynamic method agree better with the gas analyzer results [black line, Fig. 3(c)] at the beginning and end of the experiment, when the two blood samples were well separated in the tube.

To further validate the method for a systemic sO_2 change, we noninvasively imaged a mouse brain *in vivo*. The sO_2 level in the cortex was modulated by changing the oxygen concentration in the inhalation gas. Therefore, the induced sO_2 change was systemic instead of

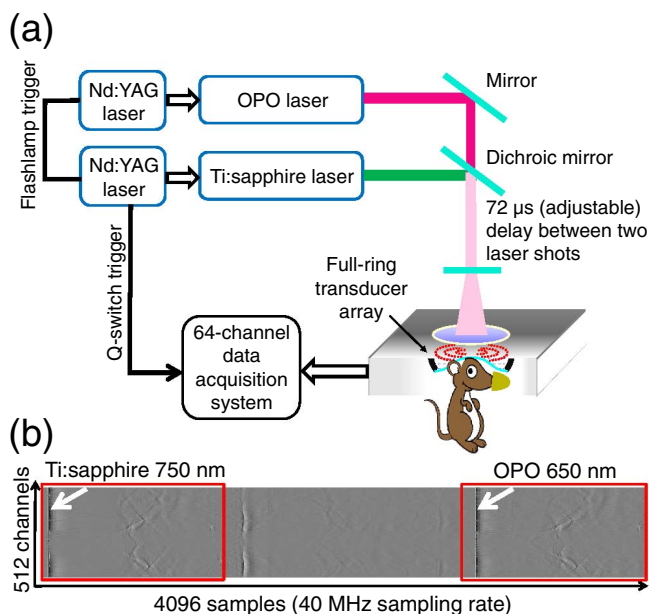


Fig. 2. (a) Schematic of the photoacoustic computed tomography system. (b) Raw channel data from the 512-element ultrasound transducer array. White arrows: photoacoustic signals generated on the transducer surface.

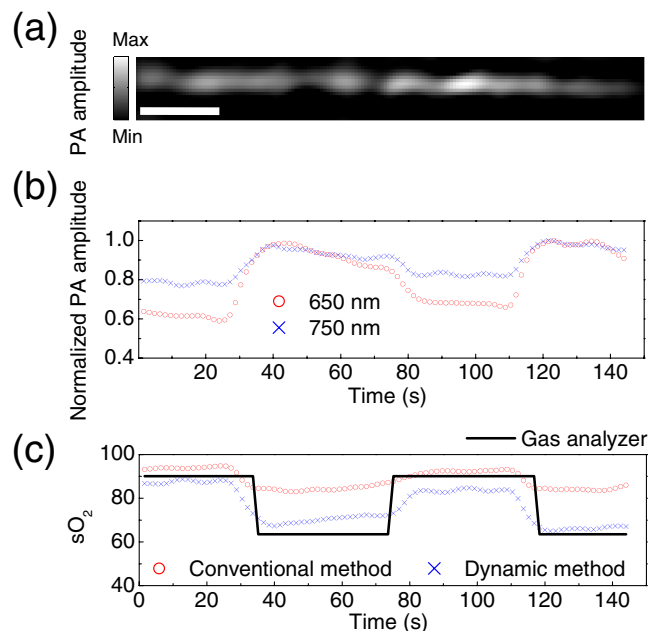


Fig. 3. Results from the phantom experiment. (a) Photoacoustic image of a blood-filled tube embedded in a piece of chicken tissue. Scale bar: 1 mm. (b). Changes in photoacoustic amplitude within the tube (Media 1, QuickTime, 5.9 MB). (c). sO_2 values calculated based on the conventional and the new dynamic methods (Media 2, QuickTime, 6.0 MB).

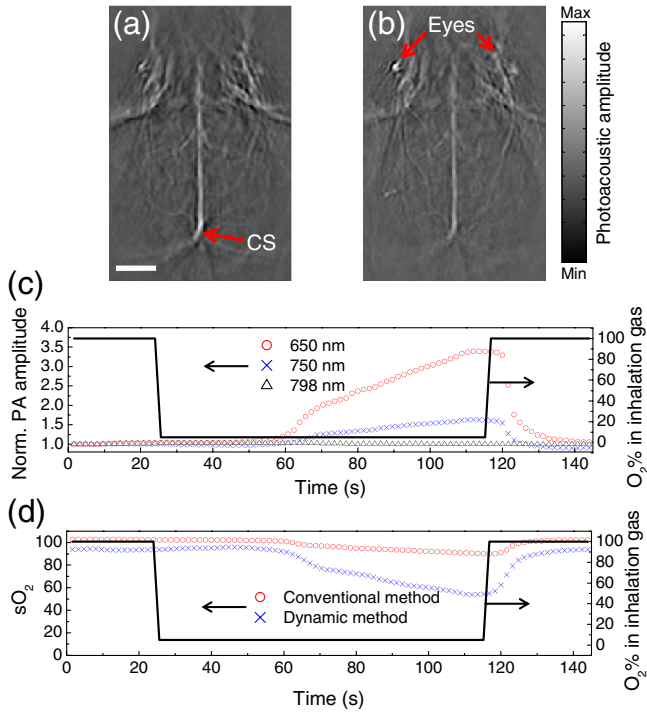


Fig. 4. *In vivo* experimental results. Photoacoustic images of cortex vasculature acquired noninvasively at (a) 650 nm and (b) 750 nm laser wavelengths. Scale bar: 2 mm. (c) Changes in photoacoustic amplitude at different wavelengths in the superior sagittal sinus. (d) sO_2 calculated based on the conventional and the new dynamic methods. (Media 3, QuickTime, 7.6 MB).

localized. However, based on the two-layer skin model presented in [17], for red and near-infrared light, the change in optical attenuation in the skin due to variations in sO_2 (e.g., from 30% to 90%) will be less than 3%, mainly because of the high scattering and low volume fraction of blood in the skin. Since the total hemoglobin concentration may change during the transition from hyperoxia to hypoxia, we also used 798 nm. Because the current system can image only two wavelengths simultaneously, the 798 nm experiment was performed in a separate scan using the same modulation protocol, and was repeated two times to ensure reproducibility.

Figures 4(a) and 4(b) show photoacoustic images of the mouse cortex vasculature acquired through the intact scalp. Because the two wavelengths have different beam profiles, the 750 nm image shows a stronger signal in the lower portion [toward the confluence of sinuses (CS)], while the 650 nm image presents a stronger signal in the upper portion [toward the mouse's eyes]. These variations will cause inaccuracy in the conventional method, but will be self-calibrated in the dynamic method. Figure 4(c) shows the average photoacoustic amplitude within the superior sagittal sinus at the three wavelengths. The photoacoustic amplitude at 798 nm remains unchanged, indicating that C_{HbT} is a constant and two wavelengths are sufficient for sO_2 calculation. The average sO_2 within the superior sagittal sinus is shown in Fig. 4(d) and Media 3. The dynamic result agrees well

with the normal range of venous sO_2 under hyperoxia and hypoxia [17]. In contrast, the conventional method generates an unrealistic sO_2 value of 100%. Based on the two-layer skin model, the differences between light attenuation at 650 and 750 nm wavelengths could be 15%, causing inaccurate sO_2 estimation.

In summary, we demonstrated the feasibility of quantifying absolute sO_2 based on the dynamics in photoacoustic signals. Instead of comparing photoacoustic amplitudes between different wavelengths, the new method analyzes photoacoustic amplitudes between different sO_2 states at each wavelength, canceling the fluence effect. The new method works well either when the sO_2 change is localized or when blood absorption is not the major light attenuation mechanism. Using PACT, the new method was demonstrated and validated in both phantom and *in vivo* experiments.

The authors appreciate Prof. James Ballard's close reading of the manuscript. This work was sponsored in part by National Institutes of Health grants DP1 EB016986 (NIH Director's Pioneer Award), R01 EB008085, R01 CA134539, U54 CA136398, R01 CA157277, and R01 CA159959. L. W. has financial interests in Microphotoacoustics, Inc. and Endra, Inc., which, however, did not support this work. Konstantin Maslov has a financial interest in Microphotoacoustics, Inc., which, however, did not support this work.

References

1. A. Cyrous, B. O'Neal, and W. D. Freeman, *Expert Rev. Neurotherap.* **12**, 915 (2012).
2. M. Hockel and P. Vaupel, *J. Natl. Cancer Inst.* **93**, 266 (2001).
3. D. Rischin, R. J. Hicks, R. Fisher, D. Binns, J. Corry, S. Porceddu, and L. J. Peters, *J. Clin. Oncol.* **24**, 2098 (2006).
4. J. Xia, M. Chatni, K. Maslov, Z. Guo, K. Wang, M. Anastasio, and L. V. Wang, *J. Biomed. Opt.* **17**, 050506 (2012).
5. M. R. Chatni, J. Xia, R. Sohn, K. Maslov, Z. Guo, Y. Zhang, K. Wang, Y. Xia, M. Anastasio, J. Arbeit, and L. V. Wang, *J. Biomed. Opt.* **17**, 076012 (2012).
6. L. V. Wang and S. Hu, *Science* **335**, 1458 (2012).
7. B. Cox, J. G. Laufer, S. R. Arridge, and P. C. Beard, *J. Biomed. Opt.* **17**, 061202 (2012).
8. J. Laufer, D. Delpy, C. Elwell, and P. Beard, *Phys. Med. Biol.* **52**, 141 (2007).
9. A. Q. Bauer, R. E. Nothdurft, T. N. Erpelding, L. V. Wang, and J. P. Culver, *J. Biomed. Opt.* **16**, 096016 (2011).
10. Z. Guo, S. Hu, and L. V. Wang, *Opt. Lett.* **35**, 2067 (2010).
11. L. Wang, S. L. Jacques, and L. Zheng, *Comput. Methods Programs Biomed.* **47**, 131 (1995).
12. D. J. Faber, F. J. van der Meer, M. C. G. Aalders, D. M. de Bruin, and T. G. van Leeuwen, *Proc. SPIE* **5861**, 58610W (2005).
13. S. Srinivasan, B. W. Pogue, S. Jiang, H. Dehghani, C. Kogel, S. Soho, J. J. Gibson, T. D. Tosteson, S. P. Poplack, and K. D. Paulsen, *Proc. Natl. Acad. Sci. U.S.A.* **100**, 12349 (2003).
14. J. Gamelin, A. Maurudis, A. Aguirre, F. Huang, P. Guo, L. V. Wang, and Q. Zhu, *Opt. Express* **17**, 10489 (2009).
15. J. Xia, Z. Guo, K. Maslov, A. Aguirre, Q. Zhu, C. Percival, and L. V. Wang, *J. Biomed. Opt.* **16**, 090505 (2011).
16. M. H. Xu and L. H. V. Wang, *Phys. Rev. E* **71**, 016706 (2005).
17. K. Maslov, H. F. Zhang, and L. V. Wang, *Inverse Probl.* **23**, S113 (2007).